Molecular Physics, Vol. 104, No. 1, 10 January 2006, 115–125

Taylor & Francis
Taylor & Francis Group

Properties of high-lying vibrational states of the H_3^+ molecular ion

JAMES J. MUNRO†, JAYESH RAMANLAL†,
JONATHAN TENNYSON*† and HAMSE Y. MUSSA‡

†Department of Physics and Astronomy, University College London,
Gower St., London WC1E 6BT
‡Unilever Centre, Chemistry Department, University of Cambridge,
Lensfield Road, Cambridge CB2 1EW, UK

(*Received 20 May 2005*)

Calculations are presented for the vibrational states of H_3^+ on a potential with the correct dissociation properties (*Molec. Phys.*, **98**, 261 (2000)) using both Radau and Jacobi coordinates. This potential is found to support horseshoe states at low to intermediate energies. Near the dissociation limit a new class of long-range states, called asymptotic vibrational states (AVS), is found. These states are similar to those suggested to explain the observed near-dissociation spectrum of H_3^+. The possible consequences of such states are discussed.

Keywords: Vibrational states; H_3^+ molecular ion

1. Introduction

The infrared near-dissociation spectrum of H_3^+ recorded by Carrington and co-workers [1–3] remains a challenge to quantum mechanical theory. Indeed, it is probably fair to say that the only aspect of this spectrum which is completely understood is its behaviour with respect to isotopic substitution, and the explanation for this rests on semi-classical rather than fully quantum mechanical analysis [4–6].

A number of studies [7–11] have calculated vibrational energy levels and wavefunctions for H_3^+ up to dissociation and, in one case, above dissociation [11]. However, these studies were all based on a non-dissociative potential energy surface which cannot be expected to give the correct behaviour for either bound or resonance states lying near the dissociation limits.

Near dissociation, one would expect the asymptotic potential of H_3^+ to display the R^{-4} behaviour associated with a proton polarizing an H_2 molecule. In the last few years a number of potential energy surfaces, which are not only more accurate in treating H_3^+ at low energies but also dissociate correctly, have been constructed [12, 13]. It is fair to assume that this long-range behaviour of the potential will influence those states of H_3^+ that lie near the dissociation limit. In this context, it is worth noting the identification of very long-range vibrational states in ozone near its dissociation limit [14] and the increased density of states observed near the dissociation limit of NO_2 [15]. A subsequent semi-classical and reduced dimension quantal calculation on NO_2 by Heiliette *et al.* [16] also demonstrated the existence of long-range states and an increased density of states at dissociation.

One of the earliest proposed explanations for the underlying structure of the coarse-grained, near-dissociation spectrum of H_3^+ was in terms of asymptotic H^+–H_2 vibration states [2, 17]. Although this explanation has generally been dropped in favour of one based on the so-called horseshoe states of the H_3^+ system [18], it is still interesting to ask whether H_3^+ does indeed support states with an unusual long-range behaviour. In this paper we report the calculation of such states; preliminary results of this study have been presented elsewhere [19].

2. Calculating the vibrational bound states of H_3^+

Accurate nuclear motion calculations were performed on Fit 2 of the global, *ab initio*, electronic ground state potential energy surface developed by Polyansky *et al.* (PPKT) [12]. This potential correctly considers the charge–polarizability interaction between H^+ and H_2

*Corresponding author. Email: j.tennyson@ucl.ac.uk

Molecular Physics
ISSN 0026–8976 print/ISSN 1362–3028 online
http://www.tandf.co.uk/journals
DOI: 10.1080/00268970500399648

at long range. This leads to a long, shallow well in the dissociation coordinate (R). A previous study of rotation–vibration states using this potential [20] had insufficient computational power to converge the near-dissociation states.

The PPKT potential energy surface was constructed to have the correct dissociative behaviour. However, closer inspection revealed that at large Jacobi R the potential exhibits an apparently unphysical hump. This hump happens to support a number of long-range states with associated classical trajectories, therefore for the purposes of this work we made slight adjustments to the potential. The PPKT potential was constructed from a number of different electronic structure calculations together with few body terms to constrain the potential at long range. The different parts of the potential were combined by using an energy switching function ($f^{\pm}(\Delta E)$) and a coordinate switching function ($g(R)$). A low-energy, high-accuracy fit (V_2) [21] was melded to a high-energy, lower-accuracy fit (V_1) using the energy switching approach of Varandas [22],

$$V_{\mathrm{ES}} = f^{+}(\Delta E)V_1(R) + f^{-}(\Delta E)V_2(R), \tag{1}$$

where the energy switching function $f^{\pm}(\Delta E)$ is

$$f^{\pm}(\Delta E) = \frac{1}{2}[1 + \tan\,\mathrm{h}(\pm\gamma\Delta E)], \tag{2}$$

with

$$\gamma = \gamma_0 + \gamma_1 \Delta E^2, \quad \Delta E = E - E_0. \tag{3}$$

The switching parameters (γ_0, γ_1, E_0) used here are the same as those used in the PPKT work [12]. We observed that the unphysical hump was coming from the second term V_2. This term was formed from high-accuracy and low-energy calculations. However, as observed in the PPKT paper [12] this term has a small but significant effect in long-range regions of the potential. This is despite the energy switching approach of equation (1). Therefore, long-range terms were also included in V_2,

$$V_2 = g(R)V_{\mathrm{SR}} + [1 - g(R)]V_{\mathrm{LR}}, \tag{4}$$

where $g(R)$ switches between the long-range (V_{LR}) and short-range (V_{SR}) terms,

$$g(R) = \begin{cases} 1, & R < R_{\mathrm{LIM}}, \\ \cos^2\left[\dfrac{\pi(R - R_{\mathrm{LIM}})}{2(R_{\mathrm{M}} - R_{\mathrm{LIM}})}\right], & R_{\mathrm{LIM}} \le R \le R_{\mathrm{M}}, \\ 0, & R > R_{\mathrm{M}}, \end{cases} \tag{5}$$

with $g(R)$ turning on at R_{LIM} and turning off at R_{M}. After a number of tests we modified just the end of the switching function R_{M} from the value of $R_{\mathrm{M}} = 10.0a_0$ to $R_{\mathrm{M}} = 7.0a_0$ and the hump disappeared. This new potential (referred to as PPKT2 in this work) is available from the corresponding author on request. We note that PPKT and PPKT2 are equal up to an energy of $30\,800\,\mathrm{cm}^{-1}$ (above the potential minimum) and a number of the calculations presented below for energies lower than this actually used the original PPKT implementation.

Full 3D Born–Oppenheimer vibrational nuclear motion calculations were performed on the ground state electronic potential surface. Here, we use a discrete variable representation (DVR) Hamiltonian matching that of the DVR3D [23] and PDVR3D [24, 25] program suites.

Calculations were performed in both Jacobi and Radau three body coordinate systems. The Radau system used here differs slightly in definition from conventional Radau coordinates, the radial coordinates stretch from the bond-length links to the position of the atom, rather than from the orthogonalization point to the atom, as is usual. This difference is necessary in order to generalize between Jacobi and Radau [26] as is done in the DVR3D program suite.

In accordance with previous calculations using PDVR3D [24] the Jacobi basis was constructed from Morse Oscillators on r and Spherical Oscillators on R. The angular basis on θ is defined as $|j\rangle = P_j(\cos\theta)$ where P_j are the usual normalized Legendre polynomials.

However, the Radau calculations required a change in the radial basis. One of the major benefits of the Radau coordinate system is that it avoids the problem of a radial coordinate going to zero at low energy with the linearity of the molecule. However, the Radau coordinate system encounters the same problem for H_3^+ but at higher energy. For this reason we used Spherical oscillators as a basis for both radial Radau coordinates. Spherical oscillators are not zero at $r = 0$ and can adequately represent wave functions with significant amplitude at $r = 0$. They are defined as [27]

$$\begin{aligned} |n\rangle &= \sqrt{2}\sqrt[4]{\beta}N_{n\alpha+(1/2)}e^{-y/2}y^{(\alpha+1)/2}L_n^{\alpha+(1/2)}(y), \\ y &= \beta r^2, \\ \beta &= \sqrt{\mu\omega_{\mathrm{e}}}, \end{aligned} \tag{6}$$

where α and ω_{e} are adjustable parameters. L_n^{α} are the usual associated Laguerre polynomials, μ is the reduced mass in the direction of r and N is the normalization constant for Laguerre polynomials.

A truncation scheme was used to reduce the basis size as much as possible. This method has been used many times before (for example, see [28]) but here is adapted for parallel operation. First, the full radial problem is solved in two dimensions for each angular grid point θ_i. The solutions to these problems are then used as an optimized two-dimensional basis for the full three-dimensional calculation. This basis can usually be significantly truncated without affecting the result tremendously and then only affecting it in a variational way.

Previous PDVR3D calculations took a constant number of basis functions from each reduced dimension calculation. This would appear to offer an easy route to parallelization as each processor could compute the 2D radial basis of a single angular grid point. Each processor then only has to truncate according to the size of basis required, no communication is required until the construction of the 3D Hamiltonian. Also, the 2D calculations should take a similar amount of time because they require the same number of solutions; the code is therefore load leveled and will perform and scale better.

This previous truncation scheme was as follows:

$$l \leq N^{2D}, \quad 1 < l < N^{\epsilon_j^{2D}}, \quad 1 < j < N^{\theta}, \tag{7}$$

where $N^{\epsilon_j^{2D}}$ is the number of solutions from each of the 2D calculations and $N^{2D} \times N^{\theta}$ gives the final Hamiltonian size. However, there are advantages to using an energy truncation scheme,

$$\epsilon_{jl}^{2D} \leq E^{2D}, \tag{8}$$

where ϵ_{jl}^{2D} are the eigenvalues from the 2D calculations and the final Hamiltonian size is not known *a priori*.

Energy is an important measure when considering the suitability of a basis function for inclusion. In our calculations we often found that an N^{2D} cut would perform no better than an energy cut with

$$E^{2D} = \max(\epsilon_{jl}^{2D}), \tag{9}$$

but at the sacrifice of a larger basis. We found that N^{3D} was often 20% larger with a number cut. So the final problem size increases and takes longer to compute but gives little return in terms of convergence.

As diagonalizers tend to scale with $O(N^3)$ for large calculations, we find that the extra 20% in the order of the Hamiltonian can double the time it takes to perform the calculation and significantly increase the memory requirements. Therefore, this energy selection scheme has been incorporated into PDVR3D.

The calculations used an adapted version of the PDVR3D code [24, 25] to perform large basis set calculations efficiently in parallel. The fully converged Radau coordinate calculations (table 1) used 384 IBM Power4+ processors for 2 h and 25 min. Calculations were performed on the HPC*x* supercomputer at the Daresbury Laboratory, UK.

The first dissociation energy of H_3^+ (D_0) corresponds to the breakup

$$H_3^+ \rightarrow H_2 + H^+, \tag{10}$$

and is therefore equal to the zero point energy of H_2. D_0 therefore differs from the classical dissociation energy D_e as any classical system would not have to achieve the zero point. In order to calculate the D_0 supported by the potential we performed a diatomic calculation using the one-dimensional potential generated by PPKT for large values of the Jacobi coordinate R and for fixed Jacobi angle θ. Using the diatomic code LEVEL7.5 [29] with this one-dimensional potential, we calculated the vibrational states of H_2. A number of cuts of the potential for various values of R and for various values of θ were tested, and we found a stable value of $D_0 = 34911.6\,\mathrm{cm}^{-1}$ relative to the ground state of H_3^+. This value is correct for both PPKT and PPKT2 as it only relies on long-range terms in the potential.

Numerical convergence of our results depends on five parameters. Three parameters control the size of the basis within our truncation scheme: N_R, N_θ and E^{2D}. Here we also refer to the final basis size (N^{3D}) calculated by using an energy cut of E^{2D}. N_R, N_θ and N^{3D} offer monotonic but not necessarily variational convergence. Two parameters control the character of the Spherical Oscillators (equation (7)): α and ω_e affect the rate of convergence.

Our main results were calculated in Radau using the PPKT2 potential energy surface. However, we also performed a number of calculations in Jacobi on the PPKT potential energy surface (some of these results are referred to below) for which we achieved good agreement up to the energy where PPKT and PPKT2 differ.

Table 1. Parameters used for converged results (Radau calculation).

Parameter	Value
N_R	120
N_θ	96
N^{3D}	79 091
α	0.0
ω_e	0.04
m/atomic mass units	1.007825

Table 2. Convergence of even parity band origins ($E(N_R)$) with respect to changes in N_R for the last 20 bound states of H_3^+. $\Delta E(N_R) = E(120) - E(N_R)$.

N_e	$E(120)$	$\Delta E(100)$	$\Delta E(105)$	$\Delta E(110)$	$\Delta E(115)$
668	34 716.850	−0.285	−0.264	−0.121	−0.040
669	34 726.958	−0.537	−0.390	−0.158	−0.082
670	34 744.139	−0.384	−0.270	−0.125	−0.028
671	34 745.815	−0.497	−0.457	−0.274	−0.098
672	34 750.744	−0.573	−0.370	−0.233	−0.084
673	34 763.433	−1.068	−0.603	−0.424	−0.170
674	34 769.659	−0.370	−0.208	−0.207	−0.060
675	34 790.860	−0.435	−0.307	−0.194	−0.081
676	34 795.457	−0.390	−0.449	−0.260	−0.092
677	34 811.712	−0.556	−0.341	−0.200	−0.090
678	34 823.961	−0.436	−0.222	−0.155	−0.082
679	34 825.222	−0.805	−0.538	−0.304	−0.114
680	34 836.529	−0.565	−0.313	−0.134	−0.027
681	34 852.006	−0.414	−0.211	−0.099	−0.051
682	34 858.105	−0.555	−0.307	−0.143	−0.094
683	34 865.425	−0.549	−0.281	−0.113	−0.014
684	34 882.977	−0.801	−0.432	−0.261	−0.126
685	34 891.348	−2.044	−1.323	−0.775	−0.270
686	34 897.999	−0.555	−0.331	−0.138	−0.142
687	34 901.023	−3.238	−2.052	−1.214	−0.544

Table 3. Convergence of even parity band origins ($E(N_\theta)$) with respect to changes in N_θ for the last 20 bound states of H_3^+. $\Delta E(N_\theta) = E(96) - E(N_\theta)$.

N_e	$E(96)$	$\Delta E(72)$	$\Delta E(80)$	$\Delta E(88)$
668	34 716.850	0.119	0.157	0.016
669	34 726.958	0.025	0.045	0.004
670	34 744.139	0.068	0.057	0.002
671	34 745.815	0.027	0.058	0.007
672	34 750.744	2.605	0.046	0.005
673	34 763.433	12.716	0.085	0.003
674	34 769.659	6.242	0.054	0.003
675	34 790.860	21.217	0.039	0.002
676	34 795.457	4.616	0.058	0.001
677	34 811.712	16.275	0.058	0.001
678	34 823.961	12.258	0.031	0.003
679	34 825.222	1.243	0.064	0.008
680	34 836.529	11.338	0.033	0.006
681	34 852.006	15.499	0.035	0.007
682	34 858.105	6.100	0.033	0.005
683	34 865.425	7.316	0.077	0.017
684	34 882.977	17.718	0.143	0.026
685	34 891.348	8.864	1.770	0.381
686	34 897.999	10.031	2.119	0.291
687	34 901.023	4.689	2.944	2.569

We find that, with the Radau calculation, all states below D_e converge to better than $0.7\,\mathrm{cm}^{-1}$ and all but one state below D_0 converge to better than $1.0\,\mathrm{cm}^{-1}$, when using the parameters given in table 1. It is possible to converge lower-energy states to much better than this but here we intentionally tried to resolve very long-range states, and this required a much larger basis and the sacrificing of some of the convergence in lower-energy states.

Table 2 shows the last 20 bound states converging with respect to the number of radial grid points (N_R). Table 3 shows the last 20 bound states converging with respect to the number of angular grid points (N_θ). Table 4 shows the last 20 bound states converging with respect to the final Hamiltonian size (N^{3D}).

Convergence was also tested by examining how the energies of states degenerate between the radial parity blocks compared. Each state was labeled with an irreducible representation (A_1, A_2, E) by examining the dot products of the wave functions with themselves under the three possible cyclic coordinate transformations. Taking $\hat{T}$ to be the cyclic transformation operator we have

$$\begin{aligned} \hat{T}\phi(r_1, r_2, \theta) &= \phi'(r_1', r_2', \theta'), \\ \hat{T}^2\phi(r_1, r_2, \theta) &= \phi''(r_1'', r_2'', \theta''), \\ \hat{T}^3\phi(r_1, r_2, \theta) &= \phi(r_1, r_2, \theta), \end{aligned} \tag{11}$$

where r_1, r_2 and θ are the Radau coordinates. We then computed the overlap integral

$$\left\langle \hat{T}\phi | \hat{T}^2\phi \right\rangle = \langle \phi' | \phi'' \rangle. \tag{12}$$

Even parity states have the property that $\langle \hat{T}\phi | \hat{T}^2\phi \rangle \approx 1$ for A_1 states and $\langle \hat{T}\phi | \hat{T}^2\phi \rangle \approx -0.5$ for E states. Combined with energy comparisons this gives a reliable method for discerning the symmetry of all the bound states. At equilibrium, this matches the permutation symmetry of the D_{3h} point group. Using this technique it was possible to clearly identify the symmetry of all but two states. States $N_e = 664$ and $N_e = 665$ differ by only $0.177\,\mathrm{cm}^{-1}$ and they appear to be of a mixed A_1,E symmetry.

The states from each parity block were then combined to give a unified list of bound states. Each state was numbered in order of energy and states degenerate across the parity block were treated as a single state. The degenerate states have their energy as an average of the separate energies. This new state numbering is referred to as N_s.

Having unified the calculations from separate parity blocks we observe that the separation in energies of degenerate states from each parity block also provides a measure of convergence. Figure 1 plots these differences

Table 4. Convergence of even parity band origins ($E(N^{3D})$) with respect to changes in N^{3D} for the last 20 bound states of H_3^+. $\Delta E(N^{3D}) = E(79\,091) - E(N^{3D})$.

N_e	E(79 091)	ΔE(59 091)	ΔE(64 091)	ΔE(69 091)	ΔE(74 091)
668	34 716.850	−0.284	−0.217	−0.103	−0.033
669	34 726.958	−0.485	−0.351	−0.190	−0.078
670	34 744.139	−0.169	−0.230	−0.078	−0.056
671	34 745.815	−0.616	−0.379	−0.202	−0.098
672	34 750.744	−0.534	−0.320	−0.160	−0.092
673	34 763.433	−0.811	−0.586	−0.349	−0.141
674	34 769.659	−0.312	−0.178	−0.147	−0.052
675	34 790.860	−0.446	−0.302	−0.116	−0.089
676	34 795.457	−0.610	−0.334	−0.243	−0.101
677	34 811.712	−0.394	−0.302	−0.149	−0.081
678	34 823.961	−0.332	−0.232	−0.117	−0.057
679	34 825.222	−0.771	−0.471	−0.280	−0.129
680	34 836.529	−0.518	−0.299	−0.120	−0.074
681	34 852.006	−0.232	−0.196	−0.090	−0.053
682	34 858.105	−0.436	−0.285	−0.152	−0.073
683	34 865.425	−0.370	−0.273	−0.129	−0.054
684	34 882.977	−0.579	−0.404	−0.244	−0.100
685	34 891.348	−0.202	−0.142	−0.070	−0.024
686	34 897.999	−0.512	−0.340	−0.182	−0.064
687	34 901.023	−0.308	−0.190	−0.107	−0.045

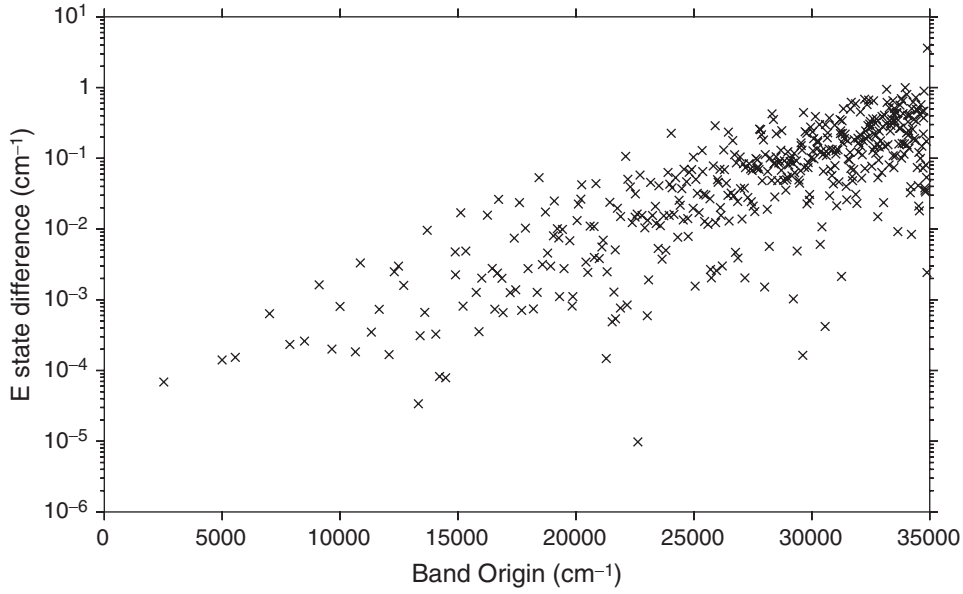

Figure 1. Comparison of energy for states degenerate across parity blocks. The energy difference is plotted on a logarithmic scale against the band origin of the same state.

on a logarithmic scale against the band origin of the same state.

With these results we found 687 even parity bound states, and 599 odd parity bound states. In terms of the irreducible representations we found 260 A_1 states, 172 A_2 states and 427 E states, wherein we have counted the degenerate E states as a single state just as with our symmetry numbering (N_s).

3. Analysis of high-lying vibrational states

One way of interpreting the nature of the high-lying vibrational states of H_3^+ is by inspection of the wave functions. However, this method is somewhat subjective as it is difficult to visualize three-dimensional wave functions and the interpretation tends to depend on the coordinate representation chosen. For this reason we

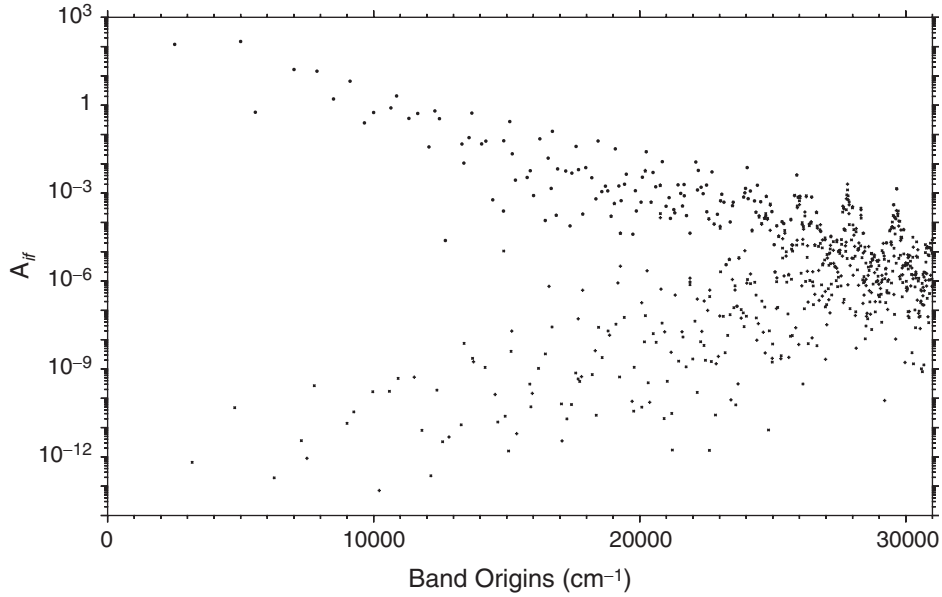

Figure 2. Einstein A_{if} coefficients for transitions to the vibrational ground state as a function of band origin.

have bolstered the wave function analysis with a calculation of other properties.

Le Sueur *et al.* [30] showed that horseshoe states have strong dipole couplings to low-lying states. They may therefore play an important part in the spectra of H_3^+. Here we repeated the same analysis, and figure 2 plots the Einstein A_{if} coefficients of all states for transitions to the vibrational ground state of H_3^+. The peaks correspond to the quantum scars of horseshoe trajectories and their nearby bath states. This calculation was performed in Jacobi coordinates using a parallel version of the dipole code (DIPOLE3) [23].

As the band origins approach dissociation the associated wave functions were found to have interesting long-range features. To understand the states of H_3^+ at high energy and to see how these states relate to the dissociation of H_3^+ we calculated expectation values for the rotational constants. To do this we used a method by Ernesti and Hutson [31] that allows expectation values of rotational constants to be calculated from the wave functions of floppy molecules given an Eckart frame.

Table 5 shows the calculated rotational constants for all states above the classical dissociation energy D_e and below the quantum dissociation energy D_0. Towards the end of this table we observe a number of states for which the rotational constant is less than expected. Here we identify 14 states with $\langle C \rangle < 7\,\mathrm{cm}^{-1}$ as asymptotic vibrational states (AVS), although calculations with even more extended radial basis sets would undoubtedly lead to further such states.

Graphical analysis was performed for all states above D_e but with particular emphasis on the identified AVS. The plots in figure 3 are DVR wave functions from the Radau calculation but plotted in Jacobi coordinates. Each Radau point was converted to Jacobi and any points lying between 89° and 91° of the Jacobi angle was included in the plot of R against r. Any Jacobi point lying between 1.3 and 1.4 of the inter-atomic r coordinate was included in the plot of R against θ.

The first three plots ($N_s = 801$, 824, 834) have a similar structure and all show no structure at all at $\theta = 90°$. This is because they are all from the odd radial parity calculation and have a node at 90°. In other states, clear nodes are visible on both the radial and angular coordinates.

In order to understand what is giving rise to these AVS and to see whether they can be understood as quantum scars of periodic classical orbits we performed a series of classical trajectory calculations including the calculations of a number of Poincaré surfaces of section.

Two-dimensional classical trajectory calculations were performed on the Jacobi coordinates r and R (at $\theta = 90°$) using the simplified classical Hamiltonian,

$$H = \frac{P_r^2}{2\mu_r} + \frac{P_R^2}{2\mu_R} + V(r, R), \tag{13}$$

where P is the momentum along a radial coordinate and μ is the reduced mass along the same coordinate. Here we use precisely the same potential V as for the quantum calculations (PPKT2) and a Fortran Runge–Kutta

Table 5. Rotational constants for all states above the classical dissociation energy (D_e). The 14 AVS states are marked in bold (identified here as states with $\langle C\rangle < 7.0\,\mathrm{cm}^{-1}$).

N_s	Band origin	γ	$\langle C\rangle$	N_s	Band origin	γ	$\langle C\rangle$	N_s	Band origin	γ	$\langle C\rangle$
682	32 832.743	E	9.139	742	33 643.759	A_1	8.737	802	34 334.312	A_1	7.175
683	32 838.584	A_1	9.263	743	33 644.020	E	8.573	803	34 356.713	E	8.256
684	32 857.022	E	9.193	744	33 656.333	A_2	8.463	804	34 371.402	A_1	8.398
685	32 859.159	E	9.219	745	33 659.176	E	8.921	805	34 377.121	A_2	8.583
686	32 874.409	A_2	8.763	746	33 669.196	A_1	9.716	806	34 383.058	E	7.563
687	32 876.224	A_1	9.898	747	33 687.240	E	8.533	807	34 412.222	E	8.376
688	32 915.384	E	8.962	748	33 712.387	E	8.933	808	34 425.456	E	8.758
689	32 916.477	A_1	8.681	749	33 717.896	A_1	8.550	809	34 440.739	E	7.940
690	32 961.061	A_1	9.207	750	33 738.596	E	8.653	810	34 458.531	A_1	7.661
691	32 962.012	E	9.152	751	33 766.310	E	8.919	811	34 473.004	A_2	7.492
692	32 977.487	E	9.104	752	33 774.187	A_2	8.787	812	34 473.552	E	7.953
693	33 005.470	E	8.948	753	33 791.886	E	8.441	813	34 479.869	A_2	7.818
694	33 012.324	A_2	9.163	754	33 801.342	A_1	9.100	814	34 487.882	E	8.257
695	33 022.487	A_1	9.289	755	33 807.867	E	8.719	815	34 509.045	A_1	8.657
696	33 041.952	A_2	8.507	756	33 818.189	A_2	8.688	816	34 514.278	E	7.876
697	33 046.078	E	9.166	757	33 831.466	E	8.867	817	34 530.009	E	8.587
698	33 048.482	A_1	9.369	758	33 833.300	A_1	8.985	818	34 530.760	A_1	8.730
699	33 078.760	E	9.491	759	33 854.800	E	9.364	819	34 537.215	E	8.034
700	33 094.601	A_1	8.986	760	33 861.541	A_1	9.193	820	34 537.704	A_2	8.085
701	33 098.350	A_2	9.051	761	33 866.317	E	8.870	821	34 560.585	E	7.973
702	33 100.299	E	9.155	762	33 889.648	A_2	8.307	822	34 578.624	A_1	8.561
703	33 121.584	A_2	9.081	763	33 892.770	A_1	8.622	823	34 595.804	E	7.910
704	33 136.403	A_1	9.316	764	33 913.458	E	9.114	**824**	**34 597.913**	**A_2**	**6.924**
705	33 147.742	A_2	8.931	765	33 913.631	A_2	8.803	825	34 606.838	E	8.728
706	33 162.403	E	8.421	766	33 931.202	E	8.274	826	34 619.147	A_1	8.365
707	33 174.989	E	9.340	767	33 954.829	A_2	8.857	827	34 633.976	E	8.167
708	33 186.704	A_1	9.692	768	33 956.829	A_1	9.248	828	34 645.934	A_2	7.864
709	33 192.039	E	9.156	769	33 961.768	E	8.556	829	34 646.539	A_1	7.650
710	33 201.243	A_2	9.493	770	33 992.400	A_1	8.509	830	34 667.981	A_1	8.498
711	33 226.285	E	8.937	771	34 009.164	A_1	8.508	831	34 668.083	E	8.384
712	33 234.119	A_1	8.970	772	34 016.768	E	8.700	832	34 677.439	E	8.581
713	33 246.551	A_2	9.043	773	34 029.107	E	8.767	833	34 685.077	A_1	7.562
714	33 275.107	E	8.875	774	34 033.467	A_1	8.880	**834**	**34 694.164**	**A_2**	**6.875**
715	33 284.878	E	8.746	775	34 038.754	A_2	8.773	835	34 711.831	A_2	8.461
716	33 315.650	A_1	8.905	776	34 042.648	E	8.892	**836**	**34 716.886**	**E**	**5.694**
717	33 329.792	E	9.172	777	34 058.184	A_2	9.044	837	34 727.068	E	8.474
718	33 347.108	A_1	9.132	778	34 066.149	E	8.561	**838**	**34 744.326**	**E**	**6.538**
719	33 352.410	E	9.110	779	34 078.049	E	8.640	839	34 745.815	A_1	8.858
720	33 361.203	A_1	10.099	780	34 079.101	E	8.699	840	34 750.977	E	8.180

(*continued*)

Table 5. Continued.

N_s	Band origin	γ	$\langle C \rangle$	N_s	Band origin	γ	$\langle C \rangle$	N_s	Band origin	γ	$\langle C \rangle$
721	33 370.986	E	9.104	781	34 082.293	A_2	8.832	841	34 762.988	E	8.689
722	33 386.455	E	9.231	782	34 103.762	E	9.369	**842**	**34 769.659**	**A_1**	**6.759**
723	33 408.141	A_1	8.981	783	34 121.110	E	7.856	843	34 790.841	E	7.728
724	33 423.080	A_2	8.791	784	34 126.874	A_1	9.234	844	34 795.439	E	7.857
725	33 435.645	E	9.529	785	34 129.533	A_2	8.789	845	34 808.455	A_2	7.461
726	33 439.955	A_2	8.852	786	34 148.197	A_1	7.527	**846**	**34 811.712**	**A_1**	**6.048**
727	33 451.474	E	9.109	787	34 158.178	E	9.043	847	34 812.020	A_2	7.816
728	33 453.888	E	8.956	788	34 159.421	A_1	9.082	848	34 823.944	E	7.233
729	33 465.606	A_1	9.016	789	34 172.314	A_1	8.889	849	34 825.222	A_1	7.343
730	33 480.188	E	8.759	790	34 176.888	E	8.859	850	34 834.888	A_2	8.548
731	33 493.204	A_2	8.457	791	34 189.886	A_2	8.767	**851**	**34 836.489**	**E**	**5.250**
732	33 507.168	E	9.173	792	34 201.917	E	8.789	**852**	**34 852.006**	**A_1**	**6.085**
733	33 513.046	A_1	9.017	793	34 227.369	E	8.869	**853**	**34 858.018**	**E**	**6.828**
734	33 520.245	E	9.309	794	34 239.662	E	8.859	**854**	**34 865.398**	**E**	**5.603**
735	33 536.546	A_1	9.354	795	34 263.257	A_1	9.554	**855**	**34 882.978**	**E**	**6.512**
736	33 548.716	E	9.004	796	34 274.747	E	8.341	**856**	**34 891.348**	**A_1**	**1.941**
737	33 578.056	A_2	8.601	797	34 294.720	A_2	8.199	857	34 897.104	A_2	8.405
738	33 585.915	E	8.712	798	34 300.868	E	8.997	858	34 897.999	A_1	7.423
739	33 590.436	A_2	8.413	799	34 313.672	A_1	8.385	**859**	**34 902.824**	**E**	**2.706**
740	33 596.613	A_1	9.177	800	34 321.463	E	8.709				
741	33 610.523	E	8.714	**801**	**34 326.376**	**A_2**	**6.976**				

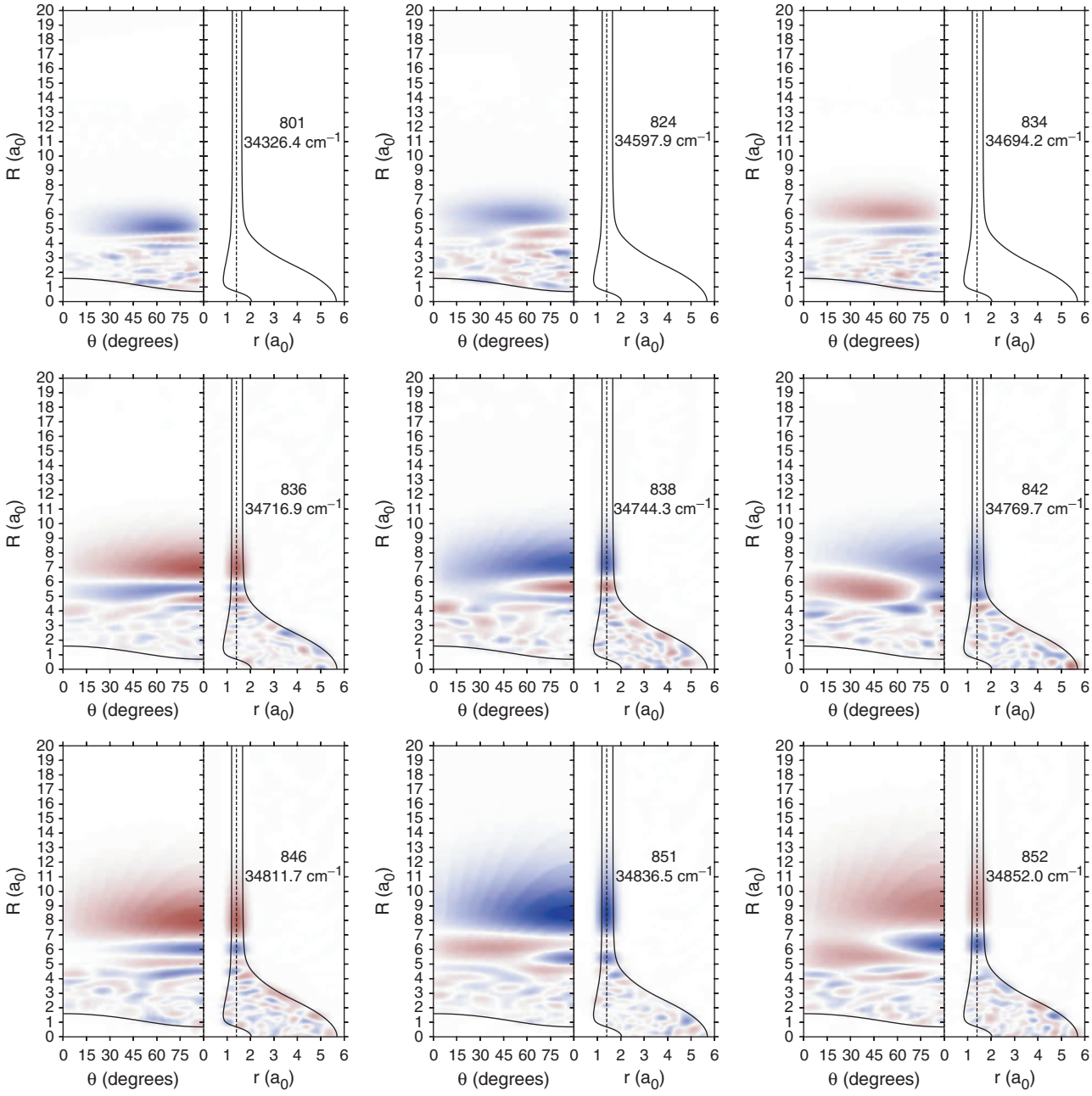

Figure 3. Two-dimensional slices through the DVR wave functions at a Jacobi angle of 90° and an inter-atomic distance of $1.4a_0$. The classical turning points for each wave function are displayed as a black contour. Wave function amplitude is plotted using a relative colour scale; each plot is scaled to the maximum amplitude within each cut of the wave function. Plots are of AVS with $\langle C \rangle < 7\,\mathrm{cm}^{-1}$.

integrator, RKSUITE [32], to compute the time evolution of a trajectory.

At low energy we find the expected trajectories for H_3^+ including the so-called horseshoe trajectories. An example horseshoe trajectory at an energy of $19\,600\,\mathrm{cm}^{-1}$ (above the potential minimum) is plotted in figure 4. At high energy the short-range trajectories become unstable and chaotic. Above the classical dissociation energy D_e the classical trajectories can also escape. Both of these types of behaviour are shown in figure 5 for a typical trajectory.

4. Conclusion

There have been many calculations on the quantal and classical behaviour of the vibrational states of H_3^+ at high energy with a view to gaining insight into

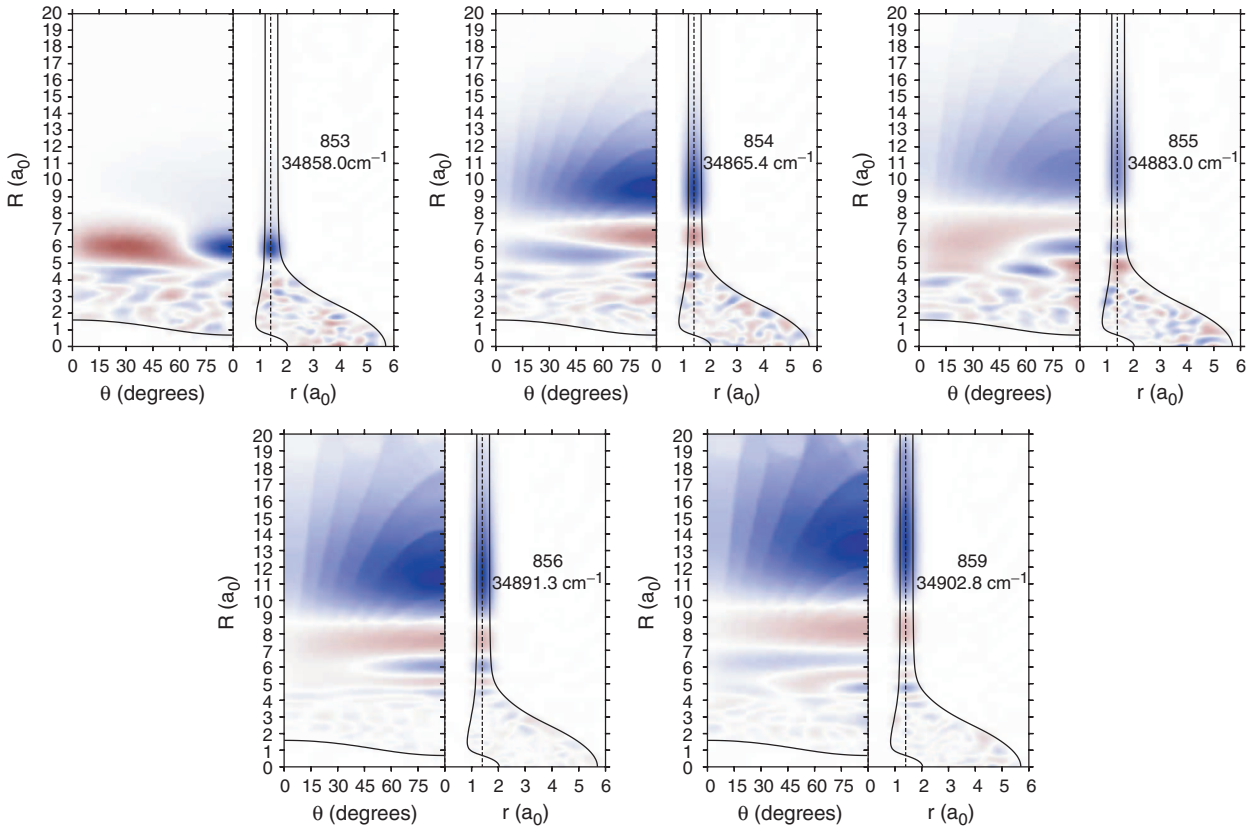

Figure 3. Continued.

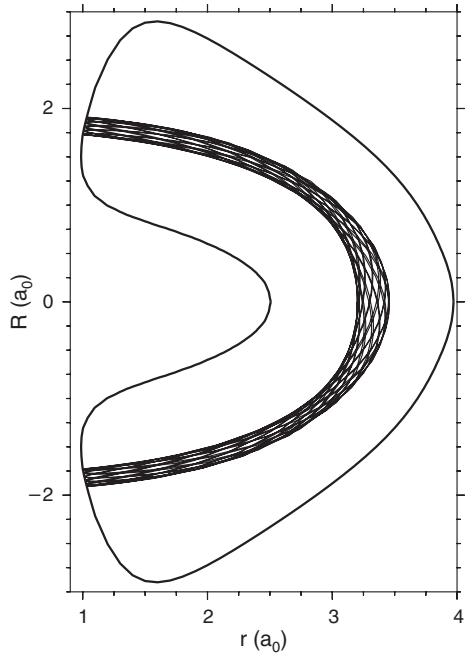

Figure 4. Plot of a classical trajectory from a stable periodic horseshoe state at an energy of 19 600 cm^{-1} (above the potential minimum). The classical turning point for the potential is shown as a thick black contour.

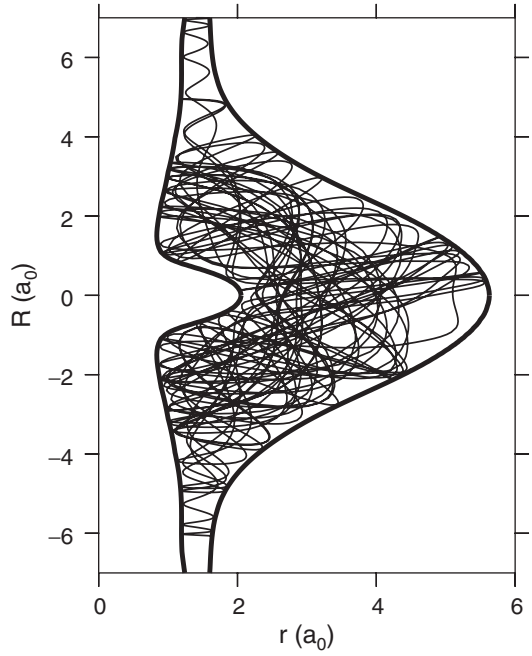

Figure 5. Plot of a typical classical trajectory at an energy of 38 000 cm^{-1} (above the potential minimum). The classical turning point of the potential is plotted as a thick black contour.

the near-dissociation spectrum of Carrington and co-workers [1–3]. However, with the exception of a poorly converged study by Kostin *et al*. [20], none of these studies used a potential energy surface with correct long-range behaviour at its dissociation limit.

Converging the vibrational wave functions for a potential with the long-range valley due to the H^+–H_2 charge–polarization interaction represents quite a challenge. We find that, as the basis set is successively extended into this valley, an increasing number of very extended vibrational states are found. We call these states asymptotic vibrational states or AVS.

It is interesting to note that, almost 20 years ago, Pfeifer and Child [17] suggested that exactly such a series of AVS could exist for H_3^+. Pfeifer and Child did this in the context of trying to find an explanation for the regular structure found at low resolution in the H_3^+ near-dissociation spectrum. Whether this really is the case will be subject of future calculations.

Acknowledgements

The authors take pleasure in acknowledging many discussions with Mark Child over many years (decades?) on the near-dissociation spectrum of H_3^+ and other topics. This article is dedicated to him and they hope he enjoys it. The authors are also grateful to Tania Monteiro for advice on the classical trajectory calculations and Paolo Barletta for helpful discussions. This work was performed as part of EPSRC's ChemReact computing consortium.

References

[1] A. Carrington, J. Buttenshaw, R.A. Kenedy. *Molec. Phys.*, **45**, 753 (1982).
[2] A. Carrington, R.A. Kennedy. *J. chem. Phys.*, **81**, 91 (1984).
[3] A. Carrington, I.R. Mcnab, Y.D. West. *J. chem. Phys.*, **98**, 1073 (1993).
[4] M. Berblinger, J.M. Gomez Llorrente, E. Pollak, C. Schlier. *Chem. Phys. Lett.*, **146**, 353 (1988).
[5] A.V. Chambers, M.S. Child. *Molec. Phys.*, **65**, 1337 (1987).
[6] M. Berblinger, E. Pollak, C. Schlier. *J. phys. Chem.*, **93**, 2319 (1989).
[7] M.J. Bramley, J.W. Tromp, T. Carrington Jr., G.C. Corey. *J. chem. Phys.*, **100**, 6175 (1994).
[8] J.R. Henderson, J. Tennyson. *Chem. Phys. Lett.*, **173**, 133 (1990).
[9] J.R. Henderson, J. Tennyson. *Molec. Phys.*, **89**, 953 (1996).
[10] J.R. Henderson, J. Tennyson, B.T. Sutcliffe. *J. chem. Phys.*, **98**, 7191 (1993).
[11] V.A. Mandelshtam, H.S. Taylor. *J. chem. Soc. Faraday Trans.*, **93**, 847 (1997).
[12] O.L. Polyansky, R. Prosmiti, W. Klopper, J. Tennyson. *Molec. Phys.*, **98**, 261 (2000).
[13] R. Prosmiti, O.L. Polyansky, J. Tennyson. *Chem. Phys. Lett.*, **273**, 107 (1997).
[14] S.Y. Grebenshcikov, R. Schinke, P. Fleurat-Lessard, M. Joyeux. *J. chem. Phys.*, **119**, 6512 (2003).
[15] R. Jost, J. Nygard, A. Pasinski, A. Delon. *J. chem. Phys.*, **105**, 1287 (1996).
[16] S. Heilliette, A. Delon, R. Jost, S. Grebenshchikov, R. Schinke, B. Abel, J.C. Rayez. *Z. phys. Chem.*, **215**, 1069 (2001).
[17] R. Pfeiffer, M.S. Child. *Molec. Phys.*, **60**, 1367 (1987).
[18] J.M. Gomez Llorente, E. Pollak. *J. chem. Phys.*, **90**, 5406 (1989).
[19] J.J. Munro, J. Ramanlal, J. Tennyson. *New J. phys.*, **7**, 196 (2005).
[20] M.A. Kostin, O.L. Polyansky, J. Tennyson, H.Y. Mussa. *J. chem. Phys.*, **118**, 3538 (2003).
[21] W. Cencek, J. Rychlewski, R. Jaquet, W. Kutzelnigg. *J. chem. Phys.*, **108**, 2831 (1998).
[22] A.J.C. Varandas. *J. chem. Phys.*, **105**, 3524 (1996).
[23] J. Tennyson, M.A. Kostin, P. Barletta, G.J. Harris, J. Ramanlal, O.L. Polyansky, N.F. Zobov. *Comput. Phys. Commun.*, 2004.
[24] H.Y. Mussa, J. Tennyson. *Comput. Phys. Commun.*, **128**, 434 (2000).
[25] J. Tennyson, P. Barletta, M.A. Kostin, O.L. Polyansky, N.F. Zobov. *Spectrochim. Acta A*, **58**, 663 (2002).
[26] B.T. Sutcliffe, J. Tennyson. *Int. J. quant. Chem.*, **39**, 183 (1991).
[27] J. Tennyson, B.T. Sutcliffe. *J. molec. Spectrosc.*, **101**, 71 (1983).
[28] Z. Bačić, J.C. Light. *A. Rev. phys. Chem.*, **40**, 469 (1989).
[29] R.J. Le Roy. LEVEL 7.5: a computer program for solving the radial Schrödinger equation for bound and quasibound levels. University of Waterloo Chemical Physics Research Report, CP-655 (2002).
[30] C.R. Le Sueur, J.R. Henderson, J. Tennyson. *Chem. Phys. Lett.*, **206**, 429 (1993).
[31] A. Ernesti, J.M. Hutson. *Chem. Phys. Lett.*, **222**, 257 (1994).
[32] R.W. Brankin, I. Gladwell, L.F. Shampine. RKSUITE: a suite of Runge–Kutta codes for the initial value problem for ODEs. Softreport 92-S1, Department of Mathematics, Southern Methodist University (1992).